Simulation of Rotary-Drum and Repose Tests for Frictional Spheres and Rigid Sphere Clusters *

O. R. Walton and R. L. Braun
Lawrence Livermore National Laboratory, Livermore, CA 94550

ABSTRACT

The effects of rotation rate and interparticle friction on the bulk flow behavior in rotating horizontal cylinders are studied via particle-dynamic simulations. Assemblies of inelastic, frictional spheres and rigid sphere clusters are utilized, and rotation rates from quasistatic to centrifuging are examined. Flow phenomena explored include size segregation, avalanching, slumping and centrifuging. Simulated drum flows with two sizes of frictional spheres showed very rapid segregation of species perpendicular to the drum axis; however, simulations of up to 10 revolutions, utilizing periodic-boundary *ends*, did not exhibit the experimentally observed axial segregation into *stripes*. Angles of repose for uniform-sized spheres in slowly rotating cylinders varied from 13 to 31 degrees as the friction coefficient varied from 0.02 to 1.0. For simulated rotation rates higher than the threshold to obtain uniform flow conditions, the apparent angle of repose increases as the rotation rate increases, consistent with experiments. Also, simulations with rigid clusters of 4 spheres in a tetrahedral shape or 8 spheres in a cubical arrangement, demonstrate that particle shape strongly influences the repose angle. Simulations of cubical 8-sphere clusters, with a surface coefficient of friction of 0.1, produced apparent angles of repose exceeding 35 degrees, compared to 23 degrees for assemblies of single spheres interacting with the same force model parameters.

Centrifuging flows at very high rotation rates exist as stationary beds moving exactly as the outer rotating wall. At somewhat slower speeds the granular bed remains in contact with the wall but exhibits surface sliding down the rising inner bed surface, moving a short distance on each revolution. At still slower speeds particles *rain* from the surface of the upper half of the rotating bed. The boundary between stationary and sliding flow is given by $\Omega^2 = 1/\sin\phi_r$, and the boundary between sliding and raining flow is approximately fit by the empirical relation $\Omega^2 = 1/\sin[\tan^{-1}(0.16 + \tan\phi_r)]$, where the non-dimensional rotation rate, Ω, is determined by $\Omega^2 = \omega_d^2 R_i/g$, and ω_d is the drum rotation rate, R_i is the radius of the inner surface of the centrifuging bed, g is the acceleration of gravity, and ϕ_r is the angle of repose for the material.

INTRODUCTION

This paper describes numerical simulations of flows of inelastic, frictional particles in rotating drums. Many industrial applications utilize rotating cylinders in processes involving granular solids and a variety of intriguing qualitative phenomena have been observed in such devices. When a slowly rotating drum is partially filled with a granular material it will usually exhibit one of two modes of motion. For very small loads (or with a very smooth interior wall) the material will initially ride up on the rising wall, then, when sufficient tangential load develops to overcome friction, the material will *slump* back down the wall, moving almost as a rigid block, with inertia usually carrying it beyond its equilibrium position. After coming to rest with respect to the outer wall, it will rise again, and repeat the cycle. For drums half or more filled (or with a rough interior wall) the material will more likely exhibit periodic surface *avalanches* down the inclined top surface. The highest attained surface angle and the lowest *slumped* surface angle often differ by as much as 10 degrees [De Jaeger, 1993]. As the rotation rate is increased,

* Work performed under the auspices of the U.S. Department of Energy by the Lawrence Livermore National Laboratory under Contract W-7405-Eng-48.

the frequency of these avalanches increases, and, when the average period between avalanches becomes less than the average duration of an individual avalanche (a time that depends on the absolute size of the drum involved and on the characteristics of the material), the material often exhibits a continuously moving top surface that has a nearly constant angle of inclination. This angle, lying somewhere between the maximum and minimum angle observed quasistatically, is often referred to as the *dynamic* or *instantaneous* angle of repose [Brown & Richards, 1970].

As the rotation rate is increased beyond the threshold *dynamic angle-of-repose* rate, inertial effects cause the flow to change character, with the upper half of the flow increasing its apparent surface angle, and the lower half decreasing its apparent surface angle. Initially the surface simply appears curved, but, at higher rotation rates, some flows appear to almost form two distinct linear surfaces [Altobelli *et al.*, 1993].

If the rotation rate is increased even further, the centrifuging limit is approached. At a rotation rate high enough to produce centrifugal force on the outer wall nearly equal to gravity, many particles appear to follow parabolic ballistic trajectories, coming off of the upper half of the rising side of the drum and falling down to a *splash* bed at the foot. True centrifuging flow, with particles remaining in continuous contact with the outer wall, requires significantly higher rotation rates than the minimum that just cancels gravity at the top of the drum. Such flows are discussed in detail later in this paper.

The qualitative flow phenomena described above are not only observed in laboratory experiments [Brown & Richards, 1970; Altobelli, *et al.* 1993], but can also be reproduced in numerical simulations of assemblies of frictional, inelastic spheres and non-spherical particles [in addition to this paper, see also: Tsuji, 1993; Ting & Corkum, 1988; Nakagawa *et al.*, 1993; Hashimoto & Watanabe, 1993]. By utilizing numerical simulation models it is possible to test sensitivity of a variety of flow phenomena to individual particle-interaction parameters such as interparticle friction or degree of inelasticity in collisions. This ability to isolate the effects of individual particle or interaction parameters can facilitate development of theories and empirical relations that focus on the most important particle characteristics. For example, simulations with a fixed coefficient of friction, independent of sliding velocity, exhibit the slumping and avalanching behaviors described above. Such simulations demonstrate that avalanching flow and periodic slumping are inherent characteristics of slowly rotating drum flows, and do not depend on *stick-slip* friction or a velocity dependent friction coefficient acting between particles or at particle-wall interfaces.

METHOD

Molecular-dynamics algorithms and methods are widely utilized and are described in several texts [Allen & Tildesley, 1987; Hockney & Eastwood, 1988; Hoover, 1991] and these same methods have been applied to macroscopic granular systems for a variety of deformation and flow conditions (see, for example Cundall & Strack [1979] and Walton [1982]). We utilize a simple, explicit, leap-frog integration algorithm (algebraically equivalent to the popular Verlet scheme) wherein positions and forces are known at the ends of each timestep and the velocities are known at the mid-point of each time-step. Newton's equations of motion are expressed as two first order differential equations in each space dimension for each particle:

$$\dot{v}_\alpha = g_\alpha + F_\alpha/m \ , \qquad \alpha = x, y, z \ ; \tag{1}$$

$$\dot{r}_\alpha = v_\alpha \ , \qquad \alpha = x,y,z \ . \tag{2}$$

These are differenced in time-centered form as:

$$v_\alpha^{n+\frac{1}{2}} = v_\alpha^{n-\frac{1}{2}} + \Delta t \left(g_\alpha + \frac{F_\alpha^n}{m} \right) \ , \quad \alpha = x,y,z \ ; \tag{3}$$

$$r_\alpha^{n+1} = r_\alpha^n + \Delta t \ v_\alpha^{n+\frac{1}{2}} \ , \qquad \alpha = x,y,z \ . \tag{4}$$

Where the superscript refers to the timestep, r is the position, v is velocity, F is the force from contacts or applied loads, m is mass, and g is the acceleration of gravity.

A radial *skin* search is employed to establish near-neighbor lists that are stored in a set of $n_p + 1$ intertwined linked lists (one list for each of the n_p particles, and a list of previously *released* memory locations that can be used for new or re-established neighbors). Individual list entries are deleted and the released memory locations are added to the *empty* list whenever a neighboring pair move further than the search distance. The entire set of neighbor lists is updated at irregular intervals, triggered by particle displacements exceeding the search radius.

Contact forces (and torques) are calculated for any near-neighbor pairs that are actually *overlapping*. The force-displacement model includes position dependent hysteresis in both the normal and tangential-friction forces. The normal-direction contact force is modeled with a linear loading (with a slope K_1) coupled with a somewhat stiffer linear unloading (with slope K_2) so that isolated, frictionless, two-body collisions will exhibit a constant coefficient of restitution, $e = \sqrt{K_1/K_2}$. The tangential force builds up (non-linearly) with finite tangential displacements after physical contact occurs. The initial slope of the tangential force displacement curve, K_{t0}, is a fixed fraction of the normal stiffness. The tangential force has a maximum value limited by the friction coefficient, μ, times the normal force. The resulting behavior is very similar to Mindlin's [1949] analysis of elastic frictional contacts between spheres. The justification for, and the details of, these force models are presented elsewhere† [Walton, 1993a,b].

The time derivatives of the angular velocities in the *principal* frame are given by Euler's equations of motion,

$$\dot{\omega}_x = \left[N_{px} + \omega_y \omega_z (I_{py} - I_{pz}) \right] / I_{px} \tag{5a}$$

$$\dot{\omega}_y = \left[N_{py} + \omega_z \omega_x (I_{pz} - I_{px}) \right] / I_{py} \tag{5b}$$

$$\dot{\omega}_z = \left[N_{pz} + \omega_x \omega_y (I_{px} - I_{py}) \right] / I_{pz} \tag{5c}$$

where $\mathbf{I}_p$ is the (diagonal) moment of inertia tensor in the principal body frame, and $\mathbf{N}_p$ is the torque vector in the principal body frame.

Because of the angular velocity products appearing on the right hand side in Equations $(5a,b,c)$ a predictor-corrector algorithm is utilized for integrating the angular velocity derivatives.

---

† Position dependent hysteretic models were employed in these *dynamic* flows to demonstrate that the effects observed do not depend on any *viscous* or *rate-dependent* parameters in the models. The simulations could have used damped harmonic oscillator (*i.e.*, spring-dashpot) models in both the normal and tangential directions with the tangential force magnitude limited by Amonton's friction rule (Friction force < μ Normal force). If such models had been utilized instead of the position-dependent hysteretic models of these simulations, the results would have been substantially equivalent to the results presented here.

The torques are known *on* the time step and the angular velocities are known at the midpoints. First, angular velocities are estimated at the current time step by assuming constant angular acceleration for an additional one-half time step,

$$\omega_\alpha'^n = \omega_\alpha^{n-\frac{1}{2}} + \Delta\omega_\alpha^{n-1}/2\,, \qquad \alpha = x,\ y,\ z\,. \tag{6}$$

These *extrapolated* angular velocities are used, along with the current torques, to make a first *prediction* of the angular accelerations at the current time step,

$$\Delta\omega_x'^n = \left[N_{px}^n + \omega_y'^n\omega_z'^n(I_{py} - I_{pz})\right]\Delta t/I_{px} \tag{7a}$$

$$\Delta\omega_y'^n = \left[N_{py}^n + \omega_z'^n\omega_x'^n(I_{pz} - I_{px})\right]\Delta t/I_{py} \tag{7b}$$

$$\Delta\omega_z'^n = \left[N_{pz}^n + \omega_x'^n\omega_y'^n(I_{px} - I_{py})\right]\Delta t/I_{pz} \tag{7c}$$

These predicted angular accelerations are then used to more accurately predict the angular velocities at the current time step,

$$\omega_\alpha^n = \omega_\alpha^{n-\frac{1}{2}} + \Delta\omega_\alpha'^n/2\,, \qquad \alpha = x,\ y,\ z. \tag{8}$$

The corrected values for the derivatives are then,

$$\Delta\omega_x^n = \left[N_{px}^n + \omega_y^n\omega_z^n(I_{py} - I_{pz})\right]\Delta t/I_{px} \tag{9a}$$

$$\Delta\omega_y^n = \left[N_{py}^n + \omega_z^n\omega_x^n(I_{pz} - I_{px})\right]\Delta t/I_{py} \tag{9b}$$

$$\Delta\omega_z^n = \left[N_{pz}^n + \omega_x^n\omega_y^n(I_{px} - I_{py})\right]\Delta t/I_{pz}. \tag{9c}$$

At this point these *corrected* values can be used directly to update angular velocities to the midpoint of the next timestep,

$$\omega_\alpha^{n+\frac{1}{2}} = \omega_\alpha^{n-\frac{1}{2}} + \Delta\omega_\alpha^n\,, \qquad \alpha = x,\ y,\ z, \tag{10}$$

or, additional iterations through the last six equations (e.g. going back to Eqn 8) can be repeated until a convergence criteria based on changes in the quantities $\Delta\omega_x^n$, $\Delta\omega_y^n$, and $\Delta\omega_z^n$ between successive iterations is satisfied, or a predetermined number of iterations is completed.

Orientaions (*i.e.*, angles) for each particle are updated using an adaptation of Evans' singularity free quaternion approach [Evans & Murad, 1977]. For Euler's equations of motion and the integration of the quaternions, the torques are specified in the *body* or *principal* frame for each non-spherical body. The contact detection and force calculations are performed in a *space* or *global* reference frame. The rotation matrix transforming from *space* to *body* frame is given by:

$$\mathbf{A} = \begin{pmatrix} -q_1^2 + q_2^2 - q_3^2 + q_4^2 & -2(q_1q_2 - q_3q_4) & 2(q_2q_3 + q_1q_4) \\ -2(q_1q_2 + q_3q_4) & q_1^2 - q_2^2 - q_3^2 + q_4^2 & -2(q_1q_3 - q_2q_4) \\ 2(q_2q_3 - q_1q_4) & -2(q_1q_3 + q_2q_4) & -q_1^2 - q_2^2 + q_3^2 + q_4^2 \end{pmatrix} \tag{11}$$

Where the q's are the quaternions of Evans and Murad [1977].

$$q_1 = \sin\tfrac{\theta}{2}\sin(\tfrac{\psi-\phi}{2})\,, \qquad q_2 = \sin\tfrac{\theta}{2}\cos(\tfrac{\psi-\phi}{2}) \tag{12a,b}$$

$$q_3 = \cos\tfrac{\theta}{2}\sin(\tfrac{\psi+\phi}{2}) \ , \qquad q_4 = \cos\tfrac{\theta}{2}\cos(\tfrac{\psi+\phi}{2}) \tag{12c,d}$$

and ϕ, θ, ψ are Euler's angles representing successive rotations about the z, x', and z' axes (see Goldstein [1950]).

The time derivatives of the orientation parameters (*i.e.*, the quaternions, q_1, q_2, q_3, q_4) can be expressed in terms of the quaternions themselves and the angular velocities [Evans & Murad, 1977],

$$\dot{q}_1 = \tfrac{1}{2}(-q_3\omega_x - q_4\omega_y + q_2\omega_z) \tag{13a}$$
$$\dot{q}_2 = \tfrac{1}{2}(q_4\omega_x - q_3\omega_y - q_1\omega_z) \tag{13b}$$
$$\dot{q}_3 = \tfrac{1}{2}(q_1\omega_x + q_2\omega_y + q_4\omega_z) \tag{13c}$$
$$\dot{q}_4 = \tfrac{1}{2}(-q_2\omega_x + q_1\omega_y - q_3\omega_z) \tag{13d}$$

Only three of the quaternions are independent and closure of this system of equations is obtained by the normalization relation,

$$\sum_{i=1}^{4} q_i^2 = 1. \tag{14}$$

Time centered finite difference versions of Eqns (13) can be solved explicitly for the quaternion values at the new time step in terms of the old values and the angular velocities at the midpoint of the timestep. The finite difference form of Eqns ($13a-d$) is,

$$q_1^{n+1} = q_1^n + \tfrac{\Delta t}{4}\left[-(q_3^{n+1}+q_3^n)\omega_x^{n+\frac{1}{2}} - (q_4^{n+1}+q_4^n)\omega_y^{n+\frac{1}{2}} + (q_2^{n+1}+q_2^n)\omega_z^{n+\frac{1}{2}}\right] \tag{15a}$$
$$q_2^{n+1} = q_2^n + \tfrac{\Delta t}{4}\left[(q_4^{n+1}+q_4^n)\omega_x^{n+\frac{1}{2}} - (q_3^{n+1}+q_3^n)\omega_y^{n+\frac{1}{2}} - (q_1^{n+1}+q_1^n)\omega_z^{n+\frac{1}{2}}\right] \tag{15b}$$
$$q_3^{n+1} = q_3^n + \tfrac{\Delta t}{4}\left[(q_1^{n+1}+q_1^n)\omega_x^{n+\frac{1}{2}} + (q_2^{n+1}+q_2^n)\omega_y^{n+\frac{1}{2}} + (q_4^{n+1}+q_4^n)\omega_z^{n+\frac{1}{2}}\right] \tag{15c}$$
$$q_4^{n+1} = q_4^n + \tfrac{\Delta t}{4}\left[-(q_2^{n+1}+q_2^n)\omega_x^{n+\frac{1}{2}} + (q_1^{n+1}+q_1^n)\omega_y^{n+\frac{1}{2}} - (q_3^{n+1}+q_3^n)\omega_z^{n+\frac{1}{2}}\right]. \tag{15d}$$

These equations can be solved for q_1^{n+1}, q_2^{n+1}, q_3^{n+1}, and q_4^{n+1}. Rearranging Eqns (15) we have,

$$q_1^{n+1} - \beta_z q_2^{n+1} + \beta_x q_3^{n+1} + \beta_y q_4^{n+1} = q_1^n + \beta_z q_2^n - \beta_x q_3^n - \beta_y q_4^n \tag{16a}$$
$$\beta_z q_1^{n+1} + q_2^{n+1} + \beta_y q_3^{n+1} - \beta_x q_4^{n+1} = -\beta_z q_1^n + q_2^n - \beta_y q_3^n + \beta_x q_4^n \tag{16b}$$
$$-\beta_x q_1^{n+1} - \beta_y q_2^{n+1} + q_3^{n+1} - \beta_z q_4^{n+1} = \beta_x q_1^n + \beta_y q_2^n + q_3^n + \beta_z q_4^n \tag{16c}$$
$$-\beta_y q_1^{n+1} + \beta_x q_2^{n+1} + \beta_z q_3^{n+1} + q_4^{n+1} = \beta_y q_1^n - \beta_x q_2^n - \beta_z q_3^n + q_4^n \tag{16d}$$

where,

$$\beta_x = \tfrac{\Delta t}{4}\omega_x^{n+\frac{1}{2}} \ , \qquad \beta_y = \tfrac{\Delta t}{4}\omega_y^{n+\frac{1}{2}} \ , \qquad \beta_z = \tfrac{\Delta t}{4}\omega_z^{n+\frac{1}{2}} \ . \tag{17a,b,c}$$

Now, let $\mathbf{B}$ be the matrix of coefficients from the left-hand side of Eqns (16) and C_i , $i = 1,2,3,4$ be the right hand sides of the four equations:

$$\mathbf{B} = \begin{pmatrix} 1 & -\beta_z & \beta_x & \beta_y \\ \beta_z & 1 & \beta_y & -\beta_x \\ -\beta_x & -\beta_y & 1 & -\beta_z \\ -\beta_y & \beta_x & \beta_z & 1 \end{pmatrix} \tag{18}$$

$$C_1 = q_1^n + \beta_z q_2^n - \beta_x q_3^n - \beta_y q_4^n \tag{19a}$$
$$C_2 = -\beta_z q_1^n + q_2^n - \beta_y q_3^n + \beta_x q_4^n \tag{19b}$$
$$C_3 = \beta_x q_1^n + \beta_y q_2^n + q_3^n + \beta_z q_4^n \tag{19c}$$
$$C_4 = \beta_y q_1^n - \beta_x q_2^n - \beta_z q_3^n + q_4^n \tag{19d}$$

Then

$$\det B = 1 + 2\beta_x^2 + 2\beta_y^2 + 2\beta_z^2 + 2\beta_x^2\beta_y^2 + 2\beta_y^2\beta_z^2 + 2\beta_x^2\beta_z^2 + \beta_x^4 + \beta_y^4 + \beta_z^4 \tag{20}$$

and

$$q_1^{n+1} = (C_1 + C_2\beta_z - C_3\beta_x - C_4\beta_y)(1 + \beta_x^2 + \beta_y^2 + \beta_z^2)/\det B \tag{21a}$$
$$q_2^{n+1} = (-C_1\beta_z + C_2 - C_3\beta_y + C_4\beta_x)(1 + \beta_x^2 + \beta_y^2 + \beta_z^2)/\det B \tag{21b}$$
$$q_3^{n+1} = (C_1\beta_x + C_2\beta_y + C_3 + C_4\beta_z)(1 + \beta_x^2 + \beta_y^2 + \beta_z^2)/\det B \tag{21c}$$
$$q_4^{n+1} = (C_1\beta_y - C_2\beta_x - C_3\beta_z + C_4)(1 + \beta_x^2 + \beta_y^2 + \beta_z^2)/\det B \tag{21d}$$

These explicit expressions for the updated q_i's are time centered (e.g., Eqns 15) and, thus avoid the additional predictor-corrector steps required by Allen and Tildesley [1987].

By their definition, Eqn (12), the quaternions satisfy the normalization relation, Eqn (14) and Evans [1977] demonstrated that Eqn (13) maintains that relation; however, to ensure that round-off error does not eventually cause normalization to fail, the resulting new quaternion values are scaled to conform with the normalization condition. A scale factor,

$$f = \left[\sum_{i=1}^{4} \left(q_i^{n+1}\right)^2\right]^{-\frac{1}{2}}, \tag{22}$$

is utilized to satisfy normalization for each particle, after each integration step,

$$q_i'^{n+1} = f q_i^{n+1}, \qquad i = 1,\ 2,\ 3,\ 4. \tag{23}$$

SIMULATIONS

Filling a vertical cylinder

Several qualitative differences in flow behavior between spheres and non-spherical particles are evidenced in simulations of particles dropping into an initially empty, vertical, right circular cylinder. In these generic simulations the ratio of loading to unloading stiffness in the normal force model (*i.e.*, K_1/K_2) is set to 0.64, corresponding to a coefficient of restitution of $e = 0.8$ for isolated collisions between spheres. For non-spherical particles the contact normal forces produce moments as well as rigid-body translational forces, so that the concept of a coefficient of restitution is somewhat less well defined. Nevertheless, the same force model parameters were used for individual contacts involving sphere clusters as for those involving single spheres. The coefficient of interparticle friction, μ, was 0.2, and the magnitude of the normal direction

stiffness was set so that the maximum *overlap* that would occur in a simulated impact would be less than one percent of a sphere diameter.

When a stream of particles falling from a height of one meter (*i.e.*, with an impact velocity of approximately $4.5m/s$) was used to fill a cylinder that was approximately 20 particle diameters across, the top of the resulting granular bed was nearly flat, as shown in Figure 1. Essentially the same surface condition was obtained whether the particles were spheres, tetrahedral clusters, cubic clusters or a mixture of the three as shown in Fig. 1. The kinetic energy imparted to the bed by each impacting particle was sufficient to vibrationally fluidize the upper surface, producing the fluid-like flat surface which remained after the vibrations attenuated. Laboratory tests of uniform sized spheres dropping into graduated cylinders can also result in flat top surfaces and, depending on both the drop height and flux, can result in a range of solid packings up to as high as 0.69 [Macrae and Gray, 1961] due to rearrangements caused, or allowed, by the energy of the impacting particles.

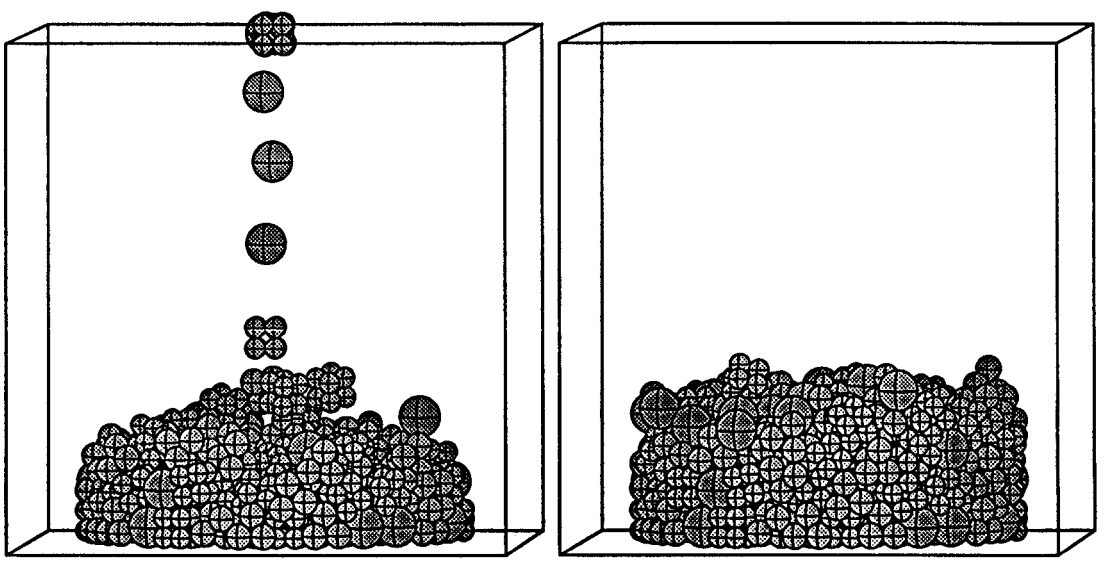

Figure 1.
Filling a right circular cylinder (not shown) with particles impacting at a velocity of $v_f \approx 4.5m/s$, $\mu = 0.2$, $e = 0.8$.

When simulated particles are dropped in a stream with a lower impact velocity (e.g., $v_f \approx 1.0m/s$) we obtain a mound under the fill stream as shown in Figures 2a and 2b. The slopes of the mounds in these two figures are significantly different, with the tetrahedral clusters forming a steeper surface than the spheres. These instantaneous snapshots of the mounds during filling are not altogether indicative of the final shape that is obtained after the fill stream is terminated. In these simulations there is sufficient kinetic energy and inertia existing near the mound peak

to allow it to flatten considerably after the fill stream is stopped. Similar inertial effects have been observed in simulations of spheres and sphere clusters by others [Hofstetter, 1993]. In experimental tests to determine angles of repose such inertial effects are usually minimized by allowing incoming particles to be quasistatically deposited from the end of a slowly raised small diameter tube (or straw) filled with the material being tested. Simulations of such angle-of-repose tests are planned.

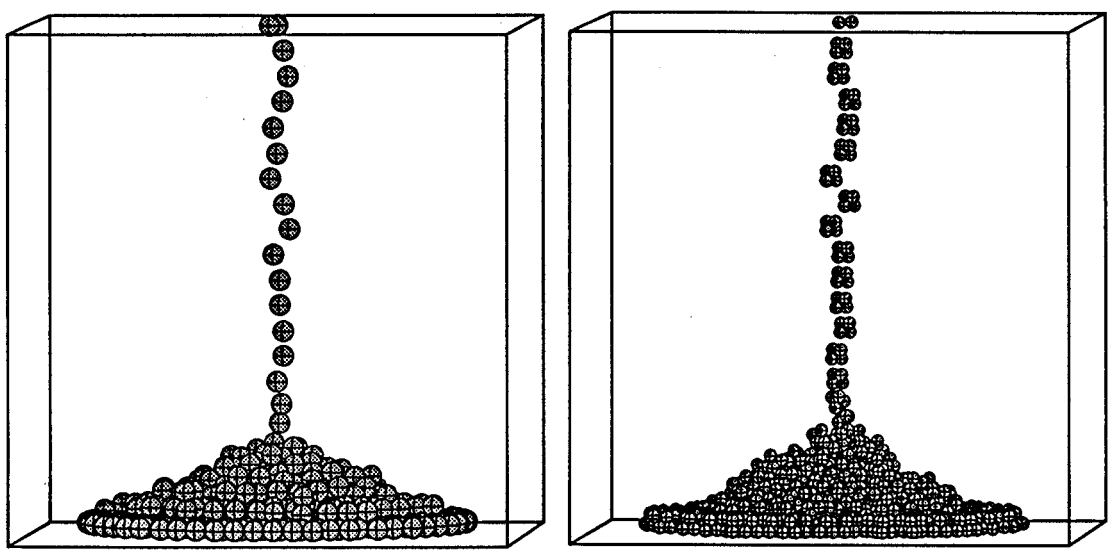

Figure 2.
Filling right circular cylinders with particles impacting at $v_f \approx 1.0m/s$, $\mu = 0.2$, $e = 0.8$, (a) spheres, and (b) sphere-clusters composed of 4 spheres in a tetrahedral arrangement.

Slowly Rotating Drums

Slumping and avalanching flows, as discussed in the introduction, are observed in simulations of very slowly rotating drums with both spheres and sphere-clusters. For the majority of the simulations discussed here the spheres were either $3mm$ (or $3.78mm$) in diameter, and the drum diameter was 42 (or 33) sphere diameters (*i.e.*, $12.6cm$). The simulation region was bounded by the rotating cylinder in the x and y directions and periodic boundaries were employed in the direction of the drum axis. The length of the cylinder section simulated was approximately 5 particle diameters (5 spheres for the single-sphere simulations, and 10 spheres for the *cubic* sphere cluster simulations).

The threshold rotation rate that produced nearly steady flows with relatively uniform inclination angles was approximately $\frac{\pi}{2}\ rad/s$. (At this rotation rate the centrifugal acceleration acting on a particle near the wall was approximately 1.5% of the gravitational acceleration, and

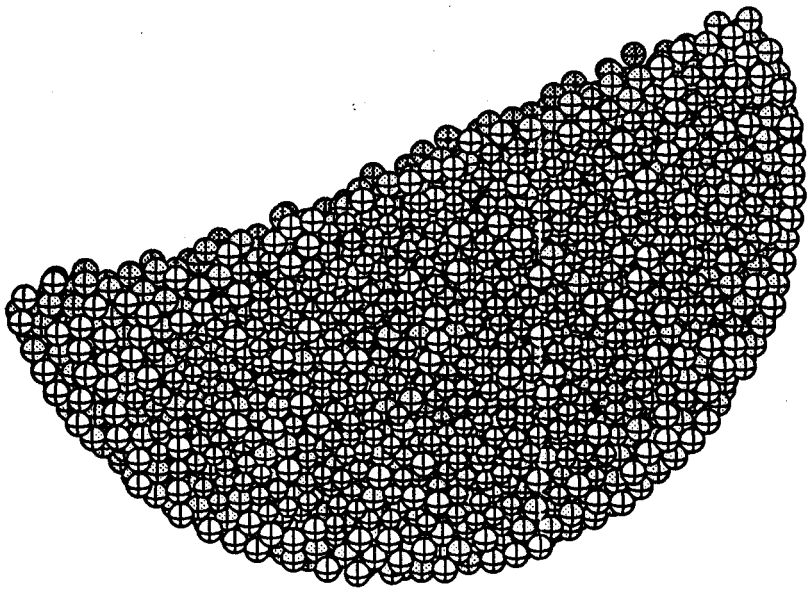

Figure 3.
Size segregation after slow partial rotation of drum containing an initially mixed assembly of $3mm$ and $3.78mm$ diameter spheres.

corresponds to a non-dimensional rotation rate, Ω_o, of 0.125, where $\Omega_o^2 = \omega_d^2 R_o/g$, ω_d is the rotation rate of the drum, R_o is the drum radius, and g is the acceleration of gravity). A variety of simulation calculations were performed at this rotation rate. Randomly mixed assemblies of two sizes of spheres, with diameters of $3mm$ and $3.78mm$ (*i.e.*, differing by a factor of 2 in volume) showed very rapid segregation in the radial drum direction. Figure 3 shows an instantaneous picture of the configuration after a rotation of just one complete revolution. The accumulation of large spheres at the toe of the incline and along the outer wall is quite evident. Similar behavior has been seen in 2-dimensional simulations of assemblies of discs [Ting & Corkum, 1988]. We obtained similar results in simulations with drums that were factors of 2 larger and smaller than the one shown in Fig. 3. These results are also consistent with the laboratory measurements of Altobelli *et al.* [1993] wherein radial direction segregation was observed to occur very rapidly in rotating drums containing binary distributions of mustard seed and also with sand.

In addition to radial segregation Nakagawa [1993] also observed segregation along the axis of the drum with alternating *stripes* of the different species appearing after several revolutions of the drum. One calculation was made to see if such *stripes* would occur in these simulated flows. The length of the simulated section was increased to approximately 50 sphere diameters, and the drum radius reduced to keep the total number of spheres at approximately 3000. After 10 simulated revolutions of the drum no axial segregation was evident. Nakagawa indicates that the segregation in his tests appears most often to originate at the ends of the drum, and he invariably obtains an odd number of stripes. The present simulations used periodic end conditions, and

thus, would not model any effects of real end walls rotating with the drum. Our very tentative conclusion is that it may be necessary to include rotating end walls in order to simulate axial segregation of binary distributions in slowly rotating drums.

Dynamic Angles of Repose

The coefficient of friction acting between particles was varied from 0.01 to 1.0 in a series of simulations examining the dynamic angle of repose of uniform sized spheres in a drum rotating at $\frac{\pi}{2}\ rad/s$. Assemblies of spheres with very low coefficients of friction (*i.e.*, $\mu = 0.01$) exhibited slumping flows, wherein the entire granular load moves almost as a block back down the rising cylinder wall, even when the drum was 2/3 filled with spheres. Increasing the friction between the wall and the spheres (while leaving the interparticle interaction parameters fixed) still resulted in periodic slumping as a rigid body. The maximum static surface angle exhibited before slumping was approximately 10 degrees. Increasing the interparticle friction coefficient resulted in nearly steady circulating flows. Table 1 summarizes the angle-of-repose simulation results.

Table 1.
Simulated angle of repose, ϕ_r, obtained in $12.6cm$ diameter rotating drum simulations with interparticle friction coefficient, μ_p, and drum rotation rate, ω_d (rad/s), for uniform $3.78mm$ diameter spheres, ○, tetrahedral sphere clusters, △, and cubic sphere clusters, □.

μ_p	ϕ_r	ω_d	Shape
0.01	10°*	$\pi/2$	○
0.02	13°	$\pi/2$	○
0.1	23°	$\pi/2$	○
0.1	25°	π	○
0.2	25°	$\pi/2$	○
1.0	31°	$\pi/2$	○
1.0	35°	π	○
0.1	28°	$\pi/2$	△
0.1	35-39°	$\pi/2$	□

*(Maximum angle before rigid body slumping)

The exact role of friction on strength of granular assemblies and on the angle of repose has been the subject of much debate in the last 100 years (see discussion in Rowe, [1962 & 1969], and Horne, [1965]). The simulation results to date do not specifically confirm any of the existing theories. This is partially because most of the theoretical treatments have been concerned with shear strength of assemblies and have ignored rolling, a mode of motion that can play a key role in the stability of the free surface of an assembly of spheres. As we explore a wider range of material properties and flow conditions we expect to be able to make comparisons to both strength and repose measurements and theories and more clearly define the role of friction on both the shear strength and the angle of repose of assemblies of particles. A significant number of additional simulation calculations will be needed before the effects of shape can be adequately

quantified. The angle of repose for the cubic sphere-clusters of the last entry in Table 1 was somewhat uncertain because of the irregular nature of the inclined top surface an example of which is shown in Figure 4.

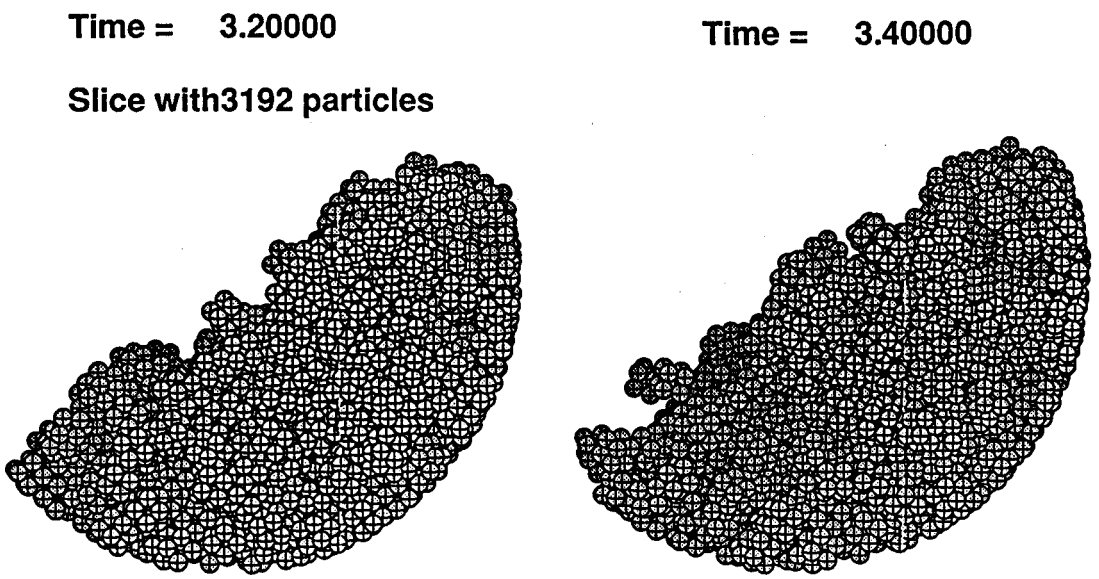

Figure 4.
Simulation with rigid 8-sphere clusters in cubical arrangement. Irregular surface makes estimate of angle of repose uncertain.

CENTRIFUGING DRUMS

When the rotation rate of a horizontal drum is fast enough for the centrifugal forces to be comparable to gravity, the character of the flow is changed considerably from the quasistatic flows discussed above. Figure 5 shows an instantaneous picture of the configuration in a simulation with a non-dimensional rotation rate, Ω_i, equal to 1.0, where $\Omega_i^2 = \omega_d^2 R_i/g$, ω_d and g are rotation rate and gavity, as before, and R_i is the radius of an imagined inner surface that would exist if all of the granular material were uniformly distributed around the circumference of the drum. At a rotation rate with $\Omega_i = 1.0$ the centrifugal force at the top of the drum just cancels gravity on a particle moving along with the outer wall, yet, as seen in Fig. 5, at this rotation rate the particles do not stay on the outer wall. Instead, they slide down the rising drum surface and also cascade in ballistic free-fall to a splash zone at the bottom of the drum. Such behavior is familiar to anyone who has run laboratory tests with granular materials in rapidly rotating drums (see, for example, Pitts [1983]). Rotation rates considerably higher than $\Omega_i = 1.0$ are required to keep a bed of granular material in continuous contact with the outer cylinder wall.

Single Frictional Particle Analysis

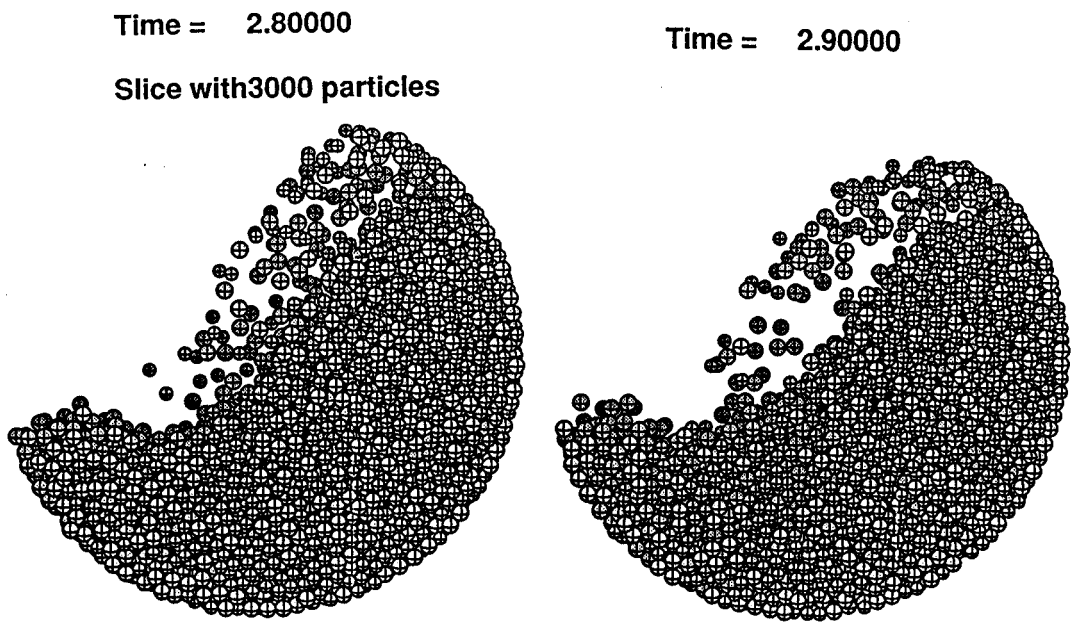

Figure 5.
Simulation of flow in a drum rotating at a rate that would cancel gravity if no slippage occurred, $\Omega_i = 1.0$. Particles interact with interparticle friction, $\mu = 0.2$, particle-wall friction, $\mu_w = 0.5$.

A simple two-body frictional contact analysis can be very useful in understanding the motion of particles on the inner surface of a centrifuging drum. Walton [1984] previously analyzed the motion of a single frictional particle on the interior frictional wall of a rotating horizontal cylinder. The numerical simulations in that previous work are essentially correct; however, the analytic form for the no-slip condition was flawed. We correct that analysis below.

The stability of particles located on the top surface of an inclined granular bed can be considered analogous to the stability of a single frictional block on an inclined plane. Whether the frictional block will remain stationary or will accelerate down the incline depends on whether the tangent of the angle of inclination of the plane is less than or greater than the coefficient of sliding friction between the block and the plane. Similarly, if the angle of inclination of a tipped granular bed exceeds the angle of repose, the top surface will flow down the incline. This is equivalent to noting that the flow is stable as long as, $\tan\alpha < \tan\phi_r$, where α is the inclination angle, ϕ_r is the angle of repose, and $\tan\alpha$ corresponds to the ratio of tangential to normal body forces due to gravity acting

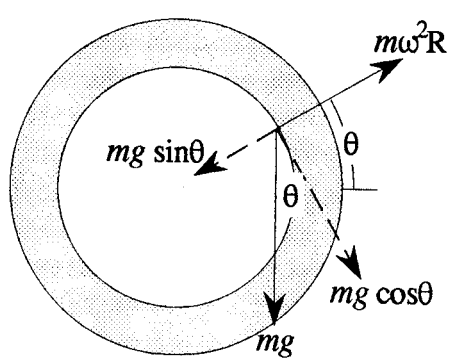

Figure 6.

on a particle on a plane inclined at the angle, α.

Extending this analogy to centrifuging flow in a horizontal rotating cylinder, we can determine the stability of a particle on the inner surface by examining the ratio of tangential to normal forces acting on it. Consider a two-dimensional view of a particle on the interior surface of a centrifuging granular bed in a rapidly rotating horizontal cylinder as shown in Figure 6, with the origin at the center of the cylinder and the polar angle, θ, measured from the horizontal. The force acting on the particle in the tangential direction, F_T, is given by

$$F_T = mg\cos\theta. \tag{24}$$

The force in the radial (*i.e.*, normal) direction, F_R, is given by

$$F_R = m\omega_d^2 R_i - mg\sin\theta, \tag{25}$$

where m is the mass of the particle, and all other variables are as previously defined. The ratio of tangential to normal force is,

$$\frac{F_T}{F_R} = \frac{\cos\theta}{\Omega_i^2 - \sin\theta} \tag{26}$$

where,

$$\Omega_i^2 = \frac{\omega_d^2 R_i}{g}, \qquad \Omega_i > 1$$

We can differentiate Eqn. (26) with respect to θ to find the location of the extrema in the force ratio,

$$\frac{d}{d\theta}\left(\frac{F_T}{F_R}\right) = \frac{(\Omega_i^2 - \sin\theta)\sin\theta - \cos^2\theta}{(\Omega_i^2 - \sin\theta)^2} = \frac{\Omega_i^2\sin\theta - 1}{(\Omega_i^2 - \sin\theta)^2}\ . \tag{27}$$

Setting this derivative to zero, we find the circumferential location, θ_{max}, where the force ratio, (F_T/F_R), is a maximum,

$$\sin\theta_{max} = \frac{1}{\Omega_i^2}\ . \tag{28}$$

Substituting this into Eqn. (26) and rearranging we obtain an expression for the maximum value of the force ratio,

$$\left.\frac{F_T}{F_R}\right|_{\theta=\theta_{max}} = \tan\theta_{max}\ . \tag{29}$$

Based on the analogy with a single frictional particle, we would expect to have a *stationary* centrifuging bed with no movement of the surface particles with respect to the rotating drum (*i.e.*, no circumferential sliding) as long as

$$\frac{F_T}{F_R} < \tan\phi_r\ , \tag{30}$$

where ϕ_r is the angle of repose for the material. The maximum value reached by the ratio F_T/F_R during each revolution of the drum is given by Eqn. (29). Thus, we will have a stationary bed if

$$\tan\theta_{max} < \tan\phi_r\ . \tag{31}$$

From which it follows that no slip will occur as long as

$$\theta_{max} < \phi_r \ , \qquad 0 < \theta_{max} < \tfrac{\pi}{2} \ , \tag{32}$$

or, combining with Eqn. (28) and rearranging, we obtain an expression for the rotation rate necessary to ensure that *no slip* occurs on the inner surface of the centrifuging granular bed,

$$\Omega_i^2 > \frac{1}{\sin \phi_r} \ . \tag{33}$$

Equation (33) defines the boundary, for cohesionless granular materials in horizontal rotating cylinders, between a stationary centrifuging bed and a granular bed exhibiting small surface slippage on each revolution. Just because surface slippage occurs, however, does not mean that particles will lose contact with the bed or *rain* down into the open central region. Numerical simulations show that surface particles can experience slippage of as much as 1/8 radian on each revolution before their tangential surface velocity becomes so low that centrifugal forces are insufficient to maintain contact with the underlying granular bed.

Walton [1984] employed a numerical integration of the motion of a single frictional block on the inside of a rotating horizontal cylinder to determine the minimum rotation rate required to keep the block in continuous contact with the cylinder. He determined the dependence of that rotation rate on the coefficient of sliding friction acting between the block and the cylinder wall. The results were fit by an empirical relation,

$$\Omega_{min}^2 = \frac{\sqrt{2}}{2}\left(1 + \frac{1}{\mu + 0.125}\right) \ . \tag{34}$$

Identifying the friction coefficient, μ, in these single particle simulations with the tangent of the angle of repose for a granular bed, $\tan \phi_r$, it was hypothesized that this same relation would represent the boundary between *sliding* and *raining* flow for a granular bed in a rotating drum,

$$\Omega_{s/r}^2 = \frac{\sqrt{2}}{2}\left(1 + \frac{1}{\tan \phi_r + 0.125}\right) \ . \tag{35}$$

This hypothesis was partially corroborated by noting a laboratory test with sand in a drum rotating at a rate just below the minimum given by Eqn. (35) exhibited particles raining from the surface [Pitts, 1983; Walton, 1984]. Here we provide another piece of corroborating evidence by simulating a drum rotating at a rate just slightly faster than the minimum given by Eqn. (35) and obtaining slipping flow with no particles raining from the surface. Figure 7 shows two instantaneous configurations from this simulation; one after 5.5 complete revolutions of the drum and the other after 14 revolutions. Particles on the inner surface in this counterclockwise rotating drum slip a short distance down the rising bed each time they pass through the *2:00o'clock* to *11:00o'clock* zone. It took nearly 10 revolutions of the drum to accelerate an initially stationary bed to the point where all *loose* particles disappeared from the central region in this simulation.

Figure 8 summarizes the results of the centrifuging and single frictional particle flow analysis and simulations. The vertical axis is the square of the non-dimensional rotation rate, Ω_i^2, and the horizontal axis is the inverse of the sine of the angle of repose, ϕ_r, (or the inverse of the

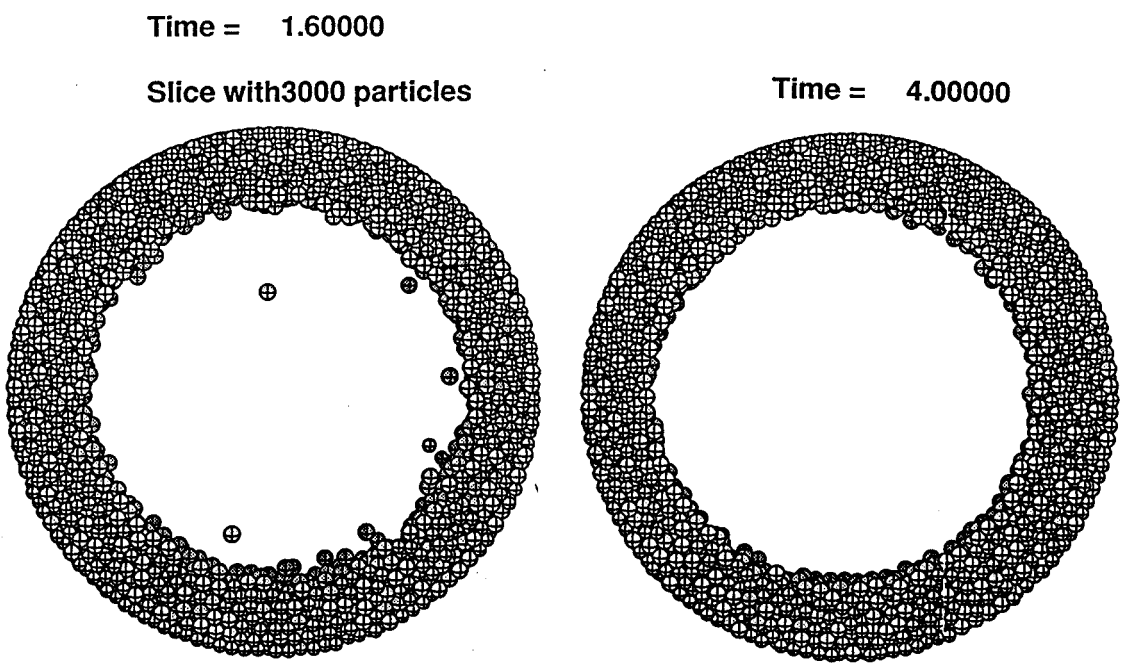

Figure 7.
Slipping flow, $\Omega_i^2 = 2.2$, $\mu = 0.2$, (a) after 5.5 revolutions of the drum and (b) after 14 complete revolutions, starting with the material stationary and the drum rotating.

sine of the friction angle for the single particle simulations). With this choice of axes, Eqn. (33) becomes a straight line demarking the boundary between stationary and sliding flows. The single particle simulations of Walton [1984], defining the boundary where particles lose contact with the wall, are plotted as open squares and triangles. The empirical curve, Eqn. (35), is shown as a dashed line. The raining sand experiment of Pitts is a filled circle and the slipping flow simulation of Fig. (7) is shown as an open circle. Also shown is the graph of an alternative empirical relationship for the bound between slipping and raining flow,

$$\Omega_{s/r}^2 = \frac{1}{\sin \phi_r'} \ , \tag{36}$$

where, ϕ_r' is an angle related to the angle of repose, ϕ_r, by the relation,

$$\tan \phi_r' = 0.16 + \tan \phi_r \ . \tag{37}$$

This empirical curve fits the majority of the single particle simulation results about as well as Eqn. (35); however, it appears to miss the last point on the right somewhat. Additional centrifuging assembly simulations are planned to test the validity of using the single particle simulation results, and thus, Eqn. (35) or (36) as the boundary between the raining and slipping flow conditions.

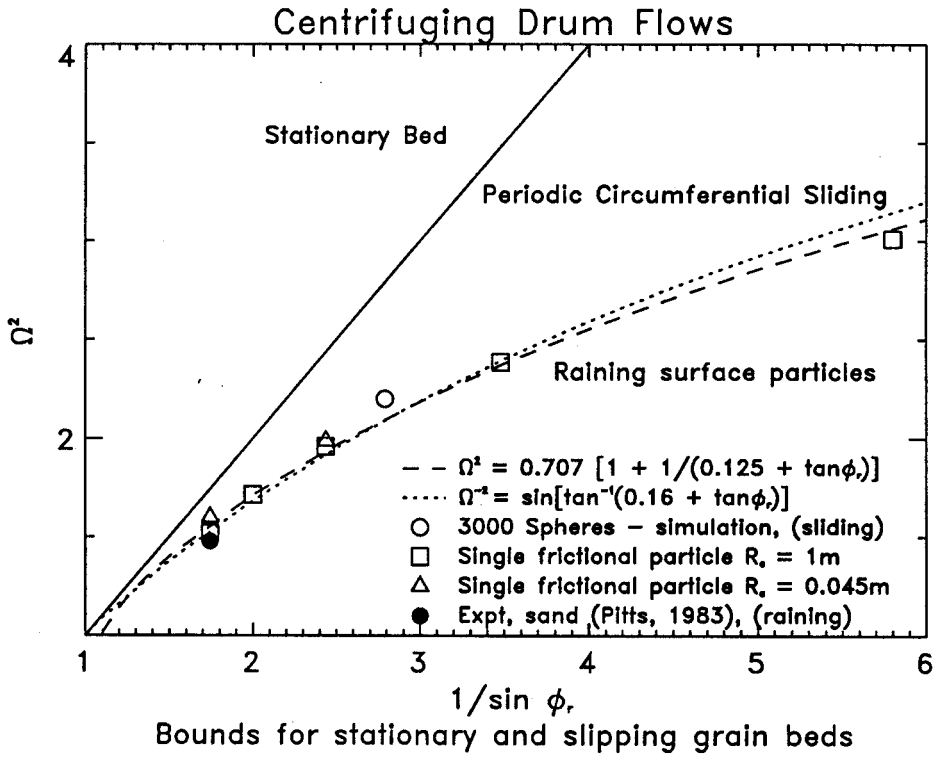

Figure 8.

CONCLUDING REMARKS

We have applied inelastic, frictional sphere models to the study of angles of repose and flows in rotating cylinders, demonstrating the significance of interparticle friction on both the angle of repose and on the slipping flow behavior in rapidly rotating drums. Analytic and empirical expressions demarking the boundaries between flow regimes in centrifuging drums are derived and/or hypothesized. These relations are consistent with experiments and simulations performed to date. We have applied the *rigid-polyatomic* approach of Evans & Murad to macroscopic granular systems and have confirmed that shape effects are as important as interparticle friction and, in some cases, are crucial to simulate in order to model observed behavior of real granular materials.

This paper is a status report of work in progress. The cylindrical outer boundary and the non-spherical particles are recent additions to our well established particle-dynamics capability. The simulations in this paper are the first exercises of those new capabilities. Some of the problems addressed here will require many additional simulation calculations in order to establish the form of expressions relating microscopic interparticle interaction parameters and measures of bulk flow behavior.

ACKNOWLEDGEMENT

This work was supported by the US Department of Energy, Office of Fossil Energy, Advanced Research and Technology Development under the Solids Transport Program administered by the Pittsburg Energy Technology Center. That support is gratefully acknowledged.

REFERENCES

Allen, M.P., and D.J. Tildesley (1987) *Computer Simulation of Liquids*, Clarendon Press, Oxford.

Altobelli, S.A., A. Caprihan, H. Cheng, E. Fukushima, M. Nakagawa, and L.Z. Wang (1993) "Progress Report: Granular Flow Studies by NMR," *DOE/NSF Workshop On Flow of Particulates and Fluids*, Plasynski, Peters, and Roco eds., Ithaca, NY.

Brown, R.L., and J.C. Richards (1970) *Principles of Powder Mechanics*, Pergamon Press, Oxford.

Cundall, P.A., and O.D.L. Strack (1979) "A Discrete Numerical Model for Granular Assemblies," *Geotechnique* **29**, 47-65.

De Jaeger, J. (1993) "Grain Shape and Size Influence on Low Stress Behavior Observing Discrete Avalanches in a Rotating Cylinder," *Powders and Grains 93*, Thornton (ed.), Balkema, rotterdam, ISBN 90 5410 323 X, p321-326.

Evans, D.J., and S. Murad (1977) "Singularity Free Algorithm for Molecular Dynamics Simulation of Rigid Polyatomics," *Mol. Phys.* **34**, p.327.

Goldstein, H. (1950) *Classical Mechanics*, Addison-Wesley.

Hashimoto, H., and R. Watanabe (1993) "Model Simulation of Impacting action of Milling Balls in Several Types of Ball Mills from Viewpoint of Mechanical Alloying," proceedings NEPTIS-1, Osaka, Japan, January 1993, Nisshin Engineering Co., Y.Tsuji, ed., p8-11.

Hockney, R.W., and J.W. Eastwood (1981) *Computer Simulation Using Particles*, McGraw-Hill, New York.

Hofstetter, K. (1993) personal communication, Caterpiller Inc., Peoria, IL.

Hoover, Wm.G. (1991) *Computational Statistical Mechanics*, Elsevier Sci. Pub., Amsterdam.

Horne, M.R. (1965) "The Behavior of an Assembly of Rotund, Rigid, Cohesionless Particles. I and II." *Proc. Roy. Soc.* **A 286**, 62 (Parts I and II); and Part III. *Proc. Roy. Soc.* **A 310**, 21-34 (1969).

Nakagawa, N., M. Hopkins, S. Altobelli, A. Caprihan, E. Fukushima, E.K. Jeong (1993) "Granular Flows in a Kiln: Non-Invasive MRI Measurements and Simulation," proceedings NEPTIS-1, Osaka, Japan, January 1993, Nisshin Engineering Co., Y.Tsuji, ed., p12-16.

Nakagawa, N. (1993) "Axial Segregation of Granular Flows in a Horizontal Rotating Cylinder," *Chem. Eng. Sci.* (Submitted).

Macrae, J.C., and W.A. Gray (1961) "Significance of the Properties of Materials in the Packing of Real Spherical particles," *Brt. J. Appl. Phys.* **12**, 164-172.

Mindlin, R.D. (1949) "Compliance of Elastic Bodies in Contact," *Trans. ASME, Series E, Journal of Appl. Mech.* **16**, 259.

Pitts, J. H., (1983) "Cascade Reactor," *Laser Program Annual Report 83*, Lawrence Livermore National Lab. Rept. UCRL-50021-83, p7-3.

Rowe, P.W. (1962) "The Stress Dilatancy Relation for Static Equilibrium of an Assembly of Particles in Contact," *Proc. Roy. Soc.*, **A 269**, 500-527.

Rowe, P.W. (1969) "Osborne Reynolds and Dilatancy," *Geotechnique* **19**, No. 1, 1-5.

Ting, J.M., and B.T. Corkum (1988) "Discrete Element Models in Geotechnical Engineering," in *Proceedings 3rd International Conference on Computing in Civil Engineering*, Vancouver, Canada, August 1988.

Tsuji, Y. (1993) private communication, Osaka, Japan.

Walton, O.R. (1982) "Explicit Particle Dynamics Model for Granular Materials," *Numerical Methods in Geomechanics*

Edmonton 1982, Z. Eisenstein, ed, A.A. Balkema, Rotterdam, Vol. 3, 1261-1268,

Walton, O.R. (1984) "Motion of Single Frictional Granules on Rotating Cylinders and Cones," *Laser Program Annual Report*, Lawrence Livermore National Laboratory Rept. UCRL-50021-84, p7.12 - 7.17.

Walton, O.R. (1993a) "Numerical Simulation of Inelastic Frictional Particle-Particle Interactions," *Particulate Two-Phase Flow* M. Roco, ed., Chap. 25, Butterworth-Heinemann, Boston.

Walton, O.R. (1993b) "Numerical Simulation of Inclined Chute Flows of Monodisperse, Inelastic, Frictional Spheres," *Mech. of Mat'ls* **16**, 239-247.